Accepted Manuscript

Accumulative fold-forging (AFF) as a novel severe plastic deformation process to fabricate a high strength ultra-fine grained layered aluminum alloy structure

F. Khodabakhshi, A.P. Gerlich

PII: S1044-5803(17)31857-0
DOI: https://doi.org/10.1016/j.matchar.2017.12.023
Reference: MTL 8972

To appear in: *Materials Characterization*

Received date: 13 July 2017
Revised date: 13 December 2017
Accepted date: 14 December 2017

Please cite this article as: F. Khodabakhshi, A.P. Gerlich , Accumulative fold-forging (AFF) as a novel severe plastic deformation process to fabricate a high strength ultra-fine grained layered aluminum alloy structure. The address for the corresponding author was captured as affiliation for all authors. Please check if appropriate. Mtl(2017), https://doi.org/10.1016/j.matchar.2017.12.023

Accumulative fold-forging (AFF) as a novel severe plastic deformation process to fabricate a high strength ultra-fine grained layered aluminum alloy structure

F. Khodabakhshi[a*] and A.P. Gerlich[b]

[a]School of Metallurgical and Materials Engineering, College of Engineering, University of Tehran, P.O. Box: 11155-4563, Tehran, Iran

[b]Department of Mechanical and Mechatronics Engineering, University of Waterloo, Waterloo, ON, Canada

[*]Corresponding author: Tel: +98 (21) 6111 4081, Fax: +98 (21) 8800 6076; E-mail: fkhodabakhshi@ut.ac.ir, farzadkhodabakhshi83@gmail.com, fkhodaba@uwaterloo.ca (F. Khodabakhshi)

Abstract

A novel severe plastic deformation (SPD) process termed accumulative fold forging (AFF) is introduced to fabricate a homogenous ultra-fine grained (UFG) layered metal structure by repetitive folding and forging aluminum alloy foil. The present work studies AFF applied to thin foils of AA8006 Al-Fe-Mn aluminum alloy after 26 folding steps to produce a UFG structure containing 67,108,864 layers across a 2 mm thickness. The structure of the layers and grain refinement are studied using X-ray diffraction (XRD), field-emission scanning electron microscopy (FE-SEM) and scanning-transmission electron microscopy (STEM) analysis. The results indicate a well-bonded inter-layer structure with an average grain size of about 200 nm parallel and 250 nm perpendicular to the forging direction, while dislocation density increased to ~7.2×10^{15} m^{-2} following AFF. The mechanical strength of the aluminum foil is evaluated in the terms of indentation hardness testing before and after AFF process. The processed UFGed layered material exhibited an average hardness value of ~61.5 Vickers

as compared to the initial value of ~30.4 Vickers for the annealed foil alloy, which indicates an improvement of ~100% due to the contributions of grain refinement, work hardening and interfacial strengthening of the bonded layers.

Keywords: Accumulative fold forging (AFF); Severe plastic deformation (SPD); AA8006 alloy; Aluminum foil; Ultra-fine grained (UFG); Indentation hardness

1. Introduction

Based on the scale of an alloy grain structure, it may be categorized into four different classes of coarse-grained (CG, larger than 10 μm), micro-crystalline (MC, larger than 1 μm), ultra-fine grained (UFG, 100-1000 nm) or nano-crystalline (NC, less than 100 nm) structures [1]. Over the last two decades, UFG and NC materials have attracted great interest considering their unique combination of mechanical properties. This largely stems from the role of grain boundaries as the main controlling structural parameter according to the well-known Hall-Petch relation [2, 3].

Two major approaches based on "bottom-up" and "top-down" strategies can be employed for processing of UFG and NC materials [1, 4]. In the first category, a solid block is formed by assembling of individual atoms or nanoparticles through different processes such as inert gas condensation [5], compaction of nano-powders [6], electro-deposition [7], melt spinning [8], and mechanical milling followed by hot/cold consolidation [9]. These are subject to many limitations for large-scale production, and have a high potential to contain residual porosity [9, 10]. However, top-down approaches are mainly based on the severe plastic deformation (SPD) concept [11, 12]. SPD methods are rooted in the intense plastic straining during particular metal-forming processes by employing a combination of shear deformation and high levels of hydrostatic pressures without any changes in the cross-sectional dimensions of the specimen. This enables grain refinement to within the UFG range through formation of high-angle grain boundaries along with increases in the dislocation density [4]. The final structure is generally free of porosity, with dimensions conducive to a wide range of testing, in which exceptional mechanical properties have been demonstrated [1, 13, 14].

To date, several SPD processes have been introduced for fabrication of UFG based metals and alloys, including; equal channel angular pressing (ECAP) [14], high pressure

torsion (HPT) [15], accumulative roll bonding (ARB) [16], simple shear extrusion (SSE) [17], accumulative spin boding (ASB) [18], twist extrusion (TE) [19], cyclic extrusion compression (CEC) [20], constrained groove pressing (CGP) [21], constrained groove rolling (CGR) [22], repetitive corrugation and straightening (RCS) [23], multi-directional forging (MDF) [24], equal channel angular rolling (ECAR) [25], friction stir processing (FSP) [26], and accumulative press bonding (APB) [27]. Among them, only the ARB and APB processes are applicable of producing UFG materials with a layered structure [28, 29]. However, limitations on the number of bonded layers as well as the imperfect bonding and strain in-homogeneities can be considered as the main drawbacks. In this research, a novel SPD process referred to as accumulative fold forging (AFF) is developed to fabricate UFGed metals and alloys with layered structure. In this new process, thin foils of metal or alloy are repetitively folded and forged (by pressing) to fabricate a high strength sheet with a layered UFG structure (see schematic representation of Fig. 1). The basic principle is similar to APB method in imposing the exceedingly large plastic shear strains on the examined material which leads to significant microstructural refinement, but there is no limitation on the number of layers which can be formed, where tens of millions can be achieved depending on the properties of the initial material. AFF is also suitable for processing of homogeneous nanocomposites and layered materials to enhance the properties and distribution of secondary phases. This process offers another advantage related to the production of thick billets, as compared to the common ARB technique for sheet metals. Also, the equipment required for the AFF process is rather simple, where only a conventional hydraulic press with two flat anvils is required.

Aluminum and its alloys have been applied in an extensive range of industrial applications in modern industries in the automotive and aerospace sectors, as a result of the unique properties offered, including a high strength to weight ratio, superior corrosion

resistance, good formability and weldability [30, 31]. For instance, the AA8XXX alloy series is an interesting category of aluminum alloys which includes additions of iron and manganese close to the Al-Fe-Mn ternary eutectic [32]. This provides an excellent combination of strength and ductility at room temperature, and allows the mechanical strength to be maintained at elevated temperatures [32, 33]. In particular, AA8006 is a well-known alloy in this series which is characterized by intermediate strength with high ductility, and contains approximately ~1.5 *wt*% and ~0.5 *wt*%, contents of iron and manganese, respectively [32]. The desirable tensile properties are attained through a uniform dispersion of fine stabilized secondary-phase dispersoids within a fine-grained Al-matrix [33]. This aluminum alloy is typically processed in the form of common household Al-foils in wide-spread use in containers, heat exchangers, air-conditioners, insulations, cable wrap and other technical applications [32, 33]. However, general applications of these Al-based materials are restricted due to their low hardness, strength and wear resistance [31]. Furthermore, if thermo-mechanical treatment is not optimized, partial recrystallization can deteriorate formability due to formation of a mixed microstructure combining coarse or elongated grains with fine equiaxed ones. Therefore, improving the mechanical properties of aluminum alloys is especially desired given the engineering challenges, and SPD concepts can be employed as an effective approach to overcome the processing deficiencies. In the case of AA8XXX aluminum series, SPD can also be effective in diminishing the processing difficulties and provide a structure with the crucially homogenous distribution of grains and precipitates, along with significant microstructural refinement to the UFG range.

The main objective of the present research is to demonstrate the AFF method as a new SPD process and assess its feasibility as a fabrication technique for production of UFG bulk material with a layered structure based on AA8006 Al-Fe-Mn alloy. The potential for aluminum alloy to accommodate fold-forging and the maximum achievable layers were

examined. Thereafter, the microstructural characteristics and mechanical properties of the fold forged material were studied by employing multiple electron microscopy analysis techniques and indentation hardness testing. Finally, the different strengthening mechanisms were assessed according to the dislocation models, and a microstructure-mechanical strength relationship was established.

2. Materials and methods

2.1 Raw materials

Commercial AA8006 aluminum foil with a thickness of 0.016 mm was used as the initial base material, and the composition was confirmed by chemical analysis according to the ASTM E1019-11, ASTM E1097-12 and ASTM E1479-16 standards by induction coupled plasma (ICP) analysis, as reported in Table 1. The contents of Fe, Mn and Si elements are in the nominal ranges as defined for the AA8006 alloy. Some foils with rectangular dimensions of 25 × 50 cm^2 and thickness of 0.016 mm were cut from the Al-foil coil and utilized as the initial samples for the AFF process.

2.2 Accumulative fold forging (AFF) process

The different stages of the AFF process are schematically illustrated in Fig. 1. This process can be performed through two consecutive steps of folding and forging. It is obvious that surface preparation is of great importance to attain reasonable metallurgical bonding between the layers as in the case of ARB and APB processes, since surface alumina oxide can be reduced by scratch brushing [28, 29]. After roughening the surface by brushing followed by degreasing within the acetone bath, the foils were carefully stacked and pressing was performed immediately to avoid from re-oxidation and further contamination. Initially, as shown in stages (I) and (II) of Fig. 1, the initial Al-foil sample was folded up to 7 times by hand to produce a compressed sample containing 128 layers. Then, it was press forged with a specific thickness reduction of about 50% in a single pass into a thickness of 2 mm by

imposing an equivalent Von-Mises plastic strain of ~0.8 by radial spreading. The pressing step was accomplished using two completely cleaned anvils without any lubrication at room temperature by using a hydraulic forming pressing machine (Macrodyne Technologies Inc, Canada) with a loading capacity of 300 tons. Thereafter, the pressed layered strip was stacked by 180 degrees via U-bending and folded, as indicated by stage (III) in Fig. 1.

This folded structure was then press forged with the same reduction ratio to enhance the previous bonds and promote bonding between the stacked layers. As a result, after an eighth folding step a structure incorporating 256 stacked layers is created (see stage (IV) in Fig. 1). By continuing this fold-forging process in further subsequent steps, it is possible to produce a multi-layered material with a homogenous structure and exceptionally high numbers of stacked layers. In this research, the process was repeated for 26 folding steps on the AA8006 aluminum foil at ambient temperature to minimize the porosity at the interfaces between layers and consequently a stacked material with UFG structure containing 67,108,864 layers was formed.

2.3 Microstructural analysis

To characterize the structural features, X-ray diffraction and electron microscopy analysis techniques were performed across the surface and thickness sections of processed layered UFGed aluminum alloy. After sample preparation according to the standard metallographic procedures by grinding and polishing along the transverse cross-section, the structure of layers and their bonding were examined by using a JSM 7600F field-emission gun scanning electron microscope (FESEM, JEOL, Japan) operating at 30 keV coupled with an energy-dispersive X-ray spectroscope (EDS) with a working distance of 15 mm and tilting angle of 70 degrees. To study the processed UFG structures, two methods of indirect calculation based on the X-ray profile broadening and direct observation with transmission electron microscopy (TEM) were employed. X-ray diffraction (XRD) analysis was performed on the surface cross-section by using a Philips X-ray diffractometer with a Cu-Kα

radiation (λ=0.154056 nm) at an angle range of 10 to 100 degree using a step width of 0.01 degrees and a counting time per step of 10 sec. A specimen with dimensions of 10×20×1.5 mm^3 was cross-sectioned parallel to the surface section and utilized for this aim. Thereafter, the measured XRD profile was evaluated by employing X'PERT software to determine the full-width at half-maximum (FWHM) of peaks for further calculations. To reveal the grain structure of the AFF processed sample, a thin foil with a thickness of less than 100 nm was sliced from the through-thickness section by the focused ion beam (FIB, JEOL, Japan) milling technique. Thereafter, the ultra-fine grain structure was observed by using a JEOL 2010F field-emission scanning/transmission electron microscope (FETEM/STEM, JEOL, Japan) operating at 200 keV. As expressed before, the morphology and distribution of precipitates are crucial to determine the mechanical properties of AA8006 aluminum alloy. Therefore, the structure of precipitates within the processed layered UFG alloy was studied by using STEM analysis, as well. TEM thin foils were prepared along the plan-view surface section by using the electrical discharge machining (EDM) technique. After thinning using standard mechanical treatments to 0.1 mm and punching a disk with 3 mm diameter, final foil perforation step was accomplished with a twin-ion milling machine (JEOL, Japan) aided by a dimpler. Observations and characterization of precipitates along the plan-view orientation were performed under the JEOL 2010F FETEM/STEM microscope.

2.4 Indentation hardness testing

Mechanical properties of processed layered material before and after AFF process was assessed by indentation hardness testing. A NANOVEA M1 Hardness Micro-indenter (NANOVEA, USA) was used for this aim. The measurements were performed across the thickness section of processed alloy. During each indent, the main parameters involved an approach load of 10 μm/min, contact load of 15 mN, applied load of 5 N, loading rate of 10 N/min, unloading rate of 10 N/min, and creep dwell times of 10 sec. These measurements

were repeated six times and the average Vickers hardness value was reported as well as the corresponding indentation load-depth graphs.

3. Results

3.1 Layered structure

To assess the bonding quality between the fold-forged AA8006 layers, FE-SEM images at different magnifications from the thickness section of the processed sample are indicated in Fig. 2. After 26 fold-forging steps, the cross-section of the final sample contains 67,108,864 layers. Also, the bright- and dark-field TEM images from a thin slice prepared by FIB lift-out across the thickness section of the sample perpendicular to the forging direction are presented in Fig. 3. Based on the SEM and TEM micrographs from the through-thickness cross-sections, these layers appear well bonded together without gaps or cracks. Considering the mentioned number of layers within a sample with thickness of 2 mm, the thickness of each layer is expected to correspond to 0.03 nm if one neglects the possibility of dynamic restoration mechanisms occurring across the layers. However, it is not possible to distinguish such interfaces between the layers through the thickness in the cross-section, which indicates excellent bonding between the folded layers without any delamination, voids, cracks or other defects. It is expected that repetitive plastic straining during such SPD process leads to the occurrence of dynamic restoration at room temperature for the examined AA8006 aluminum alloy which restricted the minimum possible grain size [34]. In the FE-SEM and FIB/TEM features from thickness cross-section, an elongated grain structure can be observed; with an UFG structure which is on average 250 nm in the through-thickness direction and 200 nm perpendicular to the forging direction (see Figs. 2 and 3).

Also, the complex precipitates incorporating Al, Fe and Mn elements are indicated as the features with white contrast in the FE-SEM images, and these will be further studied by

STEM analysis in following sections. As expressed before, the thickness of the as-received aluminum foil was about 16 μm which is several times higher than the average size of secondary phase dispersoids. Meanwhile, after the AFF process the size of precipitates is considerably larger than the apparent thickness of the stacked layers as shown in Figs. 2a and 2b. Therefore, an impingement or indentation mechanism can be considered for the precipitates between the fold-forged layers during the repeated iterations of the AFF process. Some changes in the morphology of precipitates implies the structure can undergo break-up to finer spherical inclusions, while also developing a more homogenous distribution between the layers and within the metal matrix.

3.2 Ultra-fine grained structure and precipitates

3.2.1 TEM observations and characterizations

Figures 4 and 5 show the bright- and dark-field TEM images of the grain structure of AA8006 alloy after the AFF process along the through-thickness direction of the cross-section (ie: perpendicular to the forging direction). An UFG or cellular structure with equiaxed morphology and an average size of about 250 nm is formed after multiple fold-forging steps across the thickness section. It should be noted that the ultra-fine grains are elongated perpendicular to the forging direction (see Figs. 4d,e and Figs. 5c-e).

3.2.2 Dispersoids

A main controlling parameter influencing the properties of foil products from AA8XXX series aluminum alloys is the size and distribution of particles in the microstructure, and these are mainly affected by different factors such as chemical composition, mechanical, and thermal history, including the solidification cooling rate [32, 33]. For the case of the AA8006 aluminum alloy examined here with a chemical composition of 1.5 *wt*% Fe and 0.5 *wt*% Mn, dispersoids consisting of Al_6(MnFe) and Al_3(FeMn) are the

main stable equilibrium secondary phase particles [33]. These two phases can be distinguished by their Fe:Mn ratios as 5.9:1 and 42:1, respectively. Despite the presence of some Si in the chemical composition of this alloy (~0.25 *wt*%), both phases contain negligible Si content. The most important constituent phase for this studied AA8006 aluminum alloy is Al_6(MnFe) with a mean size of around 0.5 μm and a volume fraction of 3.5% in the structure of foil product resulting from the final thermo-mechanical treatment [32, 33]. In addition, Al_3(FeMn) particles with an average size of 0.9 μm and a volume fraction of 0.8% can be considered as an another effective secondary phase precipitate, as well.

The distribution of these precipitates within the UFG structure of this aluminum alloy after the AFF process is demonstrated in Fig. 6. Also, the elemental mapping and point scan analysis results from these secondary phase dispersoid particles are presented in Figs. 7 and 8, respectively. The same phases were observed in the as-received AA8006 alloy, however the structures after AFF consist of precipitates which tend to be spherical following the applied hydrostatic pressure during the applied severe shear straining (see Figs. 6d to 6g). By comparison with the initial morphology of precipitates as reported in the literature [32, 33], some fracture and attrition of these particles to sizes less than 100-200 nm can be noticed due to the severe plastic deformation aided by the occurrence of dynamic recovery (DRV) mechanism at room temperature. These changes in the structure of precipitates are very effective in controlling the mechanical properties of the forged layered material as well as grain refinement and dislocation multiplication. According to the STEM EDS elemental mapping analysis results of Fig. 7 and point scan analysis results from precipitates in Fig. 8, both types of coarse Al_3(FeMn) (with lower fraction) and fine Al_6(MnFe) (with higher fraction) precipitates can be observed within the aluminum alloy metal-matrix.

3.3 Indentation hardness measurements

As reported in the literature [32, 33], the initial hardness of annealed AA8006 aluminum alloy is about 30.4 HV. The Vickers micro-hardness indent features across the thickness section of processed UFGed layered material and the related load-depth graphs are presented in Figs. 9 and 10, respectively. In the indentation graphs of Fig. 10, a higher penetration depth at the peak load indicates a lower hardness value. It is clear that by fabrication of UFG and layered structures the average hardness value for the AA8006 alloy is enhanced up to about 61.5 HV (see Fig. 10). Therefore, a hardness improvement of approx. 100% can be achieved. As shown in optical micro-graphs of Fig. 9, some deformation fields were generated due to anisotropy which is likely a result of the elongated grain structures observed in Figs. 3 to 5, where indentation resistance is greater along the finer grain dimension which is perpendicular to the forging direction.

4. Discussion

4.1 The effects of AFF process on the microstructural evolution

4.1.1 XRD analysis

To investigate the formation of UFG or cellular structures during SPD processes, it is useful to evaluate the broadening of XRD patterns due to imposed large plastic strains [35]. For a diffraction XRD peak, the relation between the reciprocal-space variable (S), distance between the diffraction planes (d_{hkl}), diffraction Bragg's angle (θ) and wavelength of X-ray beam (λ_x) can be expressed as follows [36]:

$$S = \frac{1}{d_{hkl}} = \frac{2\sin\theta}{\lambda_x} \tag{1}$$

Crystallite size and lattice distortion are the main two imperfections within crystalline materials which can cause X-ray peak broadening [35, 37]. Also, the structural modification can be attributed to the presence of statistical and geometrical necessary dislocations [38].

These peak broadening trends can be expressed in the terms of δS by considering the FWHMs of the main diffraction peaks. Also, a mathematical calculation based on the bell-shaped Cauchy or Gaussian functions for the broadening profiles by using the integral breadth method can be employed to separate the physical intrinsic integral breadth (δS_{phy}) from the experimental ($\delta S_{\exp}$) and instrumental profiles (δS), according to the following relationship [35, 37].

$$(\delta S)^2_{experimental} \cong (\delta S)^2_{physical} + (\delta S)^2_{instrumental} \quad (2)$$

The mentioned two grain/cell size and dislocation density effects on the X-ray line broadening due to strain anisotropy can be described by a simple superposition principle according to the modified Williamson-Hall approach as below [39]:

$$(\delta S)^2_{phy} = (\delta S^D)^2 + (\delta S^S)^2 \quad (3)$$

where δS_{phy} is the physical measured FWHM at the reciprocal lattice, δS^D is the contribution of cellular structure, and δS^D is the contribution of dislocations or micro-strain. By substituting the related relationships the following equation can be derived [37, 38]:

$$(\delta S)^2_{phy} = \left(\frac{0.9}{D}\right)^2 + \left(\frac{\pi M^2 b^2 \rho_{\exp}}{2}\right)\overline{C}_{hkl}(1 - qH^2)S^2 \quad (4)$$

$$H^2 = (h^2l^2 + k^2l^2 + h^2k^2)/(h^2 + k^2 + l^2)^2 \quad (5)$$

where D is the average grain/cell size, M is an orientation constant depending on the effective outer cut-off radius of dislocations (~1), b is the Burger's vector for the aluminum alloy (0.286 nm), $\rho_{\exp}$ is the dislocation density, $\overline{C}_{hkl}$ is an a parameter related to a diffraction plane with Miller identification of (hkl), and q is an average contrast factor depending on the type of dislocations and elastic properties of the examined aluminum alloy

[38, 40]. Consequently, by plotting $(\delta S)^2_{phy}$ versus S^2 and extrapolating this linear curve, the slope and vertical intercept yields to determination of D and ρ, respectively [40]. Figure 11a shows the typical XRD pattern for the processed UFG layered AA8006 alloy. The more intense diffraction peaks from the first four crystalline planes of (111), (200), (220) and (311) are considered for further calculations. Based on these XRD calculations, the mean cell size and dislocation density are estimated around 200 nm and 7.2×10^{15} m^{-2}, respectively (see Fig. 11b). Therefore, a good correlation can be observed between the XRD predictions and TEM observations in Figs. 4 and 5 between the grain/cell sizes.

4.1.2 Mechanism of UFG structure formation during AFF process

In the high magnification TEM images of Figs. 12a,b microstructural evolution leading to the formation of UFG structure is illustrated. Also, the mechanism for grain refinement during different stages of AFF process can be proposed as plotted in the schematic representation of Fig. 12c. At the initial steps of SPD process, dislocations are generated in a tangled orientation [4, 28]. To decrease the total strain energy of system toward the thermodynamically stable state, the initial random dislocation structure was changed to form cells by continuing the straining process as dislocation-free regions separated with dislocation-rich walls [27, 41]. Thereafter, more intense plastic deformation can lead to increases in the misorientation angle between the cells and further fragmentation to form equiaxed ultra-fine grains [1, 4]. During the fold-forging of a high stacking fault energy metal such as aluminum and its alloys, the mechanism of grain refinement is controlled by the severe shear straining as well as the dynamic recovery (DRV) phenomenon. This DRV mechanism occurs during plastic deformation of high stacking fault energy metals occurs by the multiplication, intersection and rearrangement of dislocations which leads to the formation of low-angle grain boundaries (LAGBs) as sub-grains by continuing the straining

process [1, 4]. As shown in Figs. 12a-c, clear sub-boundaries and the UFG structure are attributed to the occurrence of the DRV mechanism and short-range grain boundary migration.

4.2 Modeling of indentation hardness behavior

The multiple main strengthening mechanisms due to the contribution of grain boundaries, dislocations, precipitates and layers on the hardening behavior can be qualitatively described by using the following linear relationship as a superposition [42, 43]:

$$H = H_0 + H_{gb} + H_{dis} + H_{pp} + H_l \tag{6}$$

where H_0, H_{gb}, H_{dis}, H_{pp} and H_l are the indentation hardness due to friction effect (~4.3 Vickers), grain boundaries, dislocations, precipitates and layers, respectively. In the terms of tensile yield strength, for the UFG material these strengthening effects are explained based on the Hall-Petch relation, dislocation bow-out model and Orowan mechanism, respectively. As proposed by Khodabakhshi et al. [3], the relationship between the Vickers indentation hardness (Hv) and tensile strength (σ_{YS}) for the ultra-fine grained materials produced by SPD process can be described based on the following equation:

$$Hv_{(Vickers)} = \frac{\sigma_{YS(MPa)}}{3}(0.1)^{-n^*} \tag{7}$$

where n^* is the modified work-hardening exponent (~0.1). Therefore, the hardness of processed UFGed layered alloy can be defined as below [43, 44]:

$$H = \left(H_0 + \frac{k}{\sqrt{d}}\right) + \frac{(0.1)^{-n^*}}{3} M\tau_{cr} + \left(H_{pr} \times f_{dis}\right) + \left(f_{dfe} \times n_{il}\right) \tag{8}$$

$$\tau_{cr} = \frac{Gb}{2\pi L(1-\nu)}\left[\left(1 - \frac{3\nu}{2}\right)\ln\left(\frac{L}{b}\right) + \frac{\nu}{2} - 1\right] \tag{9}$$

where k is the proportional constant (~14.7 HV.μm$^{0.5}$), d is the mean grain size (~200 nm), M is the mean orientation or Taylor's factor (~3.06 for the FCC metals), τ_{cr} is the critical shear stress for changing the dislocations configuration to the semi-circle condition, H_{pr} is the hardness of secondary phase precipitates (~425 HV), f_{dis} is the precipitates distribution (shape and volume fraction) effect, d_{dfe} is the deformation field effect due to the presence of layers with arrester orientation and corresponding anisotropy influence, n_{il} is the number of layers located under the indenter during indentation testing, G is the shear modulus of aluminum matrix (~25.9 GPa), b is the Burger's vector (~0.286 nm), L is the average dislocation length ($\cong \frac{C}{\sqrt{\rho}}$), and ν is the Poisson's ratio (~0.33) [43, 45]. By summarizing, the following general equation can be derived [43, 45]:

$$H = H_y + \frac{(0.1)^{-n^*}}{3}\frac{GbM\sqrt{\rho}}{2\pi C(1-\nu)}\left[\left(1-\frac{3\nu}{2}\right)\ln\left(\frac{C}{b\sqrt{\rho}}\right)+\frac{\nu}{2}-1\right]+H_{pr}\left[\frac{V_p(s+2)}{2}-V_p\right]+f_{dfe}\left(\frac{d_{ind}}{t}n_l\right) \quad (10)$$

where H_y is the yielding hardness ($\cong\left(H_0+\frac{k}{\sqrt{d}}\right)$), C is a proportional constant (~0.9), ρ is the dislocation density (~7.2×10^{15} m^{-2}), V_p is the volume fraction of secondary phase complex $Al_6(MnFe)$ and $Al_3(FeMn)$ precipitates (~4.3 *vol*%), s is the aspect ratio of these dispersoids (~1), d_{ind} is the indentation diamond diagonal (~0.13-0.14 mm), t is the sample thickness (~2 mm), and n_l is the number of stacked layers after AFF process (~67,108,864) [43]. For estimating the hardness strengthening effect due to the presence of layered structure and subsequent generated strain fields, this relationship was used and f_{dfe} value determined about 2×10^{-6} as expressed in Table 2.

5. Concluding remarks

A novel SPD process was invented for manufacturing of UFGed layered materials. This AFF method was implemented successfully on an AA8006 alloy up to 26 cycles by repetitive folding and forging stages. The microstructural features and mechanical properties of processed layered structure were investigated by XRD, FE-SEM, TEM, STEM and indentation hardness testing. A considerable volume fraction of $(FeMn)Al_6$ precipitates was observed within the grain structure of examined Al-Fe-Mn alloy. As a result, fabrication of 67,108,864 stacked layers at a thickness of ~2 mm and occurrence of dynamic restoration at low temperature can restrict the mean grain size less than <250 nm along the forging direction. Also, a good bonding between this massive numbers of layers was attained. However, the SPD straining and dynamic recovery leads to the formation of a well-developed UFG structure consisting of high-angle grain boundaries with an average grain size of ~200 nm parallel to the surface plane and a dislocation density of around 7.2×10^{15} m^{-2}. The indentation hardness improved from an initial value of ~30.4 Vickers for the annealed foil alloy up to ~61.5 HV, after AFF process. The theoretical models revealed the important contributions of strain hardening, grain refinement and layered structure strengthening's on this significant two times hardening effect.

Acknowledgements:

The authors would like to acknowledge the financial support of the Natural Sciences and Engineering Research Council of Canada (NSERC). Access to pressing facilities was greatly appreciated courtesy of Prof. Michael Worswick.

References

[1] R.Z. Valiev, R.K. Islamgaliev, I.V. Alexandrov, Bulk nanostructured materials from severe plastic deformation, *Prog. Mater Sci.* 45(2) (2000) 103-189.

[2] S.H.C. Park, Y.S. Sato, H. Kokawa, Microstructural evolution and its effect on Hall-Petch relationship in friction stir welding of thixomolded Mg alloy AZ91D, *J. Mater. Sci.* 38(21) (2003) 4379-4383.

[3] F. Khodabakhshi, M. Haghshenas, H. Eskandari, B. Koohbor, Hardness−strength relationships in fine and ultra-fine grained metals processed through constrained groove pressing, *Mater. Sci. Eng., A* 636 (2015) 331-339.

[4] L.S. Toth, C. Gu, Ultrafine-grain metals by severe plastic deformation, *Mater. Charact.* 92 (2014) 1-14.

[5] N. Chen, D.V. Louzguine-Luzgin, K. Yao, A new class of non-crystalline materials: Nanogranular metallic glasses, *J. Alloys Compd.* 707 (2017) 371-378.

[6] R. Birringer, H. Gleiter, H.P. Klein, P. Marquardt, Nanocrystalline materials an approach to a novel solid structure with gas-like disorder?, *Physics Letters A* 102(8) (1984) 365-369.

[7] M.H. Chakrabarti, C.T.J. Low, N.P. Brandon, V. Yufit, M.A. Hashim, M.F. Irfan, J. Akhtar, E. Ruiz-Trejo, M.A. Hussain, Progress in the electrochemical modification of graphene-based materials and their applications, *Electrochim. Acta* 107 (2013) 425-440.

[8] L.H. Zhang, X.P. Duan, X. Yan, M. Yu, X. Ning, Y. Zhao, Y.Z. Long, Recent advances in melt electrospinning, *RSC Advances* 6(58) (2016) 53400-53414.

[9] C. Suryanarayana, N. Al-Aqeeli, Mechanically alloyed nanocomposites, *Prog. Mater Sci.* 58(4) (2013) 383-502.

[10] C. Suryanarayana, Mechanical alloying and milling, *Prog. Mater Sci.* 46(1–2) (2001) 1-

184.

[11] A.K. Gupta, T.S. Maddukuri, S.K. Singh, Constrained groove pressing for sheet metal processing, *Prog. Mater Sci.* 84 (2016) 403-462.

[12] P. Kumar, M. Kawasaki, T.G. Langdon, Review: Overcoming the paradox of strength and ductility in ultrafine-grained materials at low temperatures, *J. Mater. Sci.* 51(1) (2016) 7-18.

[13] M. Kawasaki, Different models of hardness evolution in ultrafine-grained materials processed by high-pressure torsion, *J. Mater. Sci.* 49(1) (2014) 18-34.

[14] R.Z. Valiev, T.G. Langdon, Principles of equal-channel angular pressing as a processing tool for grain refinement, *Prog. Mater Sci.* 51(7) (2006) 881-981.

[15] A.P. Zhilyaev, T.G. Langdon, Using high-pressure torsion for metal processing: Fundamentals and applications, *Prog. Mater Sci.* 53(6) (2008) 893-979.

[16] Y. Saito, H. Utsunomiya, N. Tsuji, T. Sakai, Novel ultra-high straining process for bulk materials-development of the accumulative roll-bonding (ARB) process, *Acta Mater.* 47(2) (1999) 579-583.

[17] N. Pardis, R. Ebrahimi, Deformation behavior in Simple Shear Extrusion (SSE) as a new severe plastic deformation technique, *Mater. Sci. Eng., A* 527(1–2) (2009) 355-360.

[18] M.S. Mohebbi, A. Akbarzadeh, Accumulative spin-bonding (ASB) as a novel SPD process for fabrication of nanostructured tubes, *Mater. Sci. Eng., A* 528(1) (2010) 180-188.

[19] Y. Beygelzimer, V. Varyukhin, S. Synkov, D. Orlov, Useful properties of twist extrusion, *Mater. Sci. Eng., A* 503(1–2) (2009) 14-17.

[20] N. Pardis, B. Talebanpour, R. Ebrahimi, S. Zomorodian, Cyclic expansion-extrusion (CEE): A modified counterpart of cyclic extrusion-compression (CEC), *Mater. Sci. Eng., A*

528(25–26) (2011) 7537-7540.

[21] D.H. Shin, J.J. Park, Y.S. Kim, K.T. Park, Constrained groove pressing and its application to grain refinement of aluminum, *Mater. Sci. Eng., A* 328(1–2) (2002) 98-103.

[22] J.W. Lee, J.J. Park, Numerical and experimental investigations of constrained groove pressing and rolling for grain refinement, *J. Mater. Process. Technol.* 130–131 (2002) 208-213.

[23] J. Huang, Y.T. Zhu, D.J. Alexander, X. Liao, T.C. Lowe, R.J. Asaro, Development of repetitive corrugation and straightening, *Mater. Sci. Eng., A* 371(1–2) (2004) 35-39.

[24] D.G. Morris, M.A. Muñoz-Morris, High creep strength, dispersion-strengthened iron aluminide prepared by multidirectional high-strain forging, *Acta Mater.* 58(18) (2010) 6080-6089.

[25] Y.Q. Cheng, Z.H. Chen, W.J. Xia, Drawability of AZ31 magnesium alloy sheet produced by equal channel angular rolling at room temperature, *Mater. Charact.* 58(7) (2007) 617-622.

[26] R.S. Mishra, Z.Y. Ma, Friction stir welding and processing, *Mater. Sci. Eng., R* 50(1–2) (2005) 1-78.

[27] S. Amirkhanlou, M. Ketabchi, N. Parvin, S. Khorsand, R. Bahrami, Accumulative press bonding; a novel manufacturing process of nanostructured metal matrix composites, *Mater. Des.* 51 (2013) 367-374.

[28] S. Amirkhanlou, M. Ketabchi, N. Parvin, M. Askarian, F. Carreño, Achieving ultrafine grained and homogeneous AA1050/ZnO nanocomposite with well-developed high angle grain boundaries through accumulative press bonding, *Mater. Sci. Eng., A* 627 (2015) 374-380.

[29] S.O. Gashti, A. Fattah-alhosseini, Y. Mazaheri, M.K. Keshavarz, Microstructure, mechanical properties and electrochemical behavior of AA1050 processed by accumulative roll bonding (ARB), *J. Alloys Compd.* 688, Part B (2016) 44-55.

[30] J.C. Benedyk, 3 - Aluminum alloys for lightweight automotive structures A2 - Mallick, P.K, Materials, Design and Manufacturing for Lightweight Vehicles, Woodhead Publishing 2010, pp. 79-113.

[31] G.S. Cole, A.M. Sherman, Light weight materials for automotive applications, *Mater. Charact.* 35(1) (1995) 3-9.

[32] O. Engler, G. Laptyeva, N. Wang, Impact of homogenization on microchemistry and recrystallization of the Al-Fe-Mn alloy AA 8006, *Mater. Charact.* 79 (2013) 60-75.

[33] P. Moldovan, G. Popescu, F. Miculescu, Microscopic study regarding the microstructure evolution of the 8006 alloy in the plastic deformation process, *J. Mater. Process. Technol.* 153-154(1-3) (2004) 408-415.

[34] T. Sakai, A. Belyakov, R. Kaibyshev, H. Miura, J.J. Jonas, Dynamic and post-dynamic recrystallization under hot, cold and severe plastic deformation conditions, *Prog. Mater Sci.* 60 (2014) 130-207.

[35] J. He, J. Ye, E.J. Lavernia, D. Matejczyk, C. Bampton, J.M. Schoenung, Quantitative analysis of grain size in bimodal powders by X-ray diffraction and transmission electron microscopy, *J. Mater. Sci.* 39(23) (2004) 6957-6964.

[36] F. Khodabakhshi, M. Kazeminezhad, The effect of constrained groove pressing on grain size, dislocation density and electrical resistivity of low carbon steel, *Mater. Des.* 32(6) (2011) 3280-3286.

[37] H.G. Jiang, M. Rühle, E.J. Lavernia, On the applicability of the X-ray diffraction line profile analysis in extracting grain size and microstrain in nanocrystalline materials, *J. Mater.*

Res. 14(2) (1999) 549-559.

[38] Z. Zhang, F. Zhou, E.J. Lavernia, On the analysis of grain size in bulk nanocrystalline materials via X-ray diffraction, *Metall. Mater. Trans. A* 34 A(6) (2003) 1349-1355.

[39] T. Ungár, J. Gubicza, G. Ribárik, A. Borbély, Crystallite size distribution and dislocation structure determined by diffraction profile analysis: principles and practical application to cubic and hexagonal crystals, *J. Appl. Crystallogr.* 34(3) (2001) 298-310.

[40] P. Scardi, M. Leoni, R. Delhez, Line broadening analysis using integral breadth methods: A critical review, *J. Appl. Crystallogr.* 37(3) (2004) 381-390.

[41] Y. Estrin, A. Vinogradov, Extreme grain refinement by severe plastic deformation: A wealth of challenging science, *Acta Mater.* 61(3) (2013) 782-817.

[42] F. Khodabakhshi, A. Simchi, A.H. Kokabi, P. Švec, F. Simančík, A.P. Gerlich, Effects of nanometric inclusions on the microstructural characteristics and strengthening of a friction-stir processed aluminum–magnesium alloy, *Mater. Sci. Eng., A* 642 (2015) 215-229.

[43] N. Hansen, Hall–Petch relation and boundary strengthening, *Scr. Mater.* 51(8) (2004) 801-806.

[44] F. Khodabakhshi, A. Simchi, A.H. Kokabi, A.P. Gerlich, M. Nosko, Effects of post-annealing on the microstructure and mechanical properties of friction stir processed Al–Mg–TiO_2 nanocomposites, *Mater. Des.* 63 (2014) 30-41.

[45] Z. Zhang, D.L. Chen, Consideration of Orowan strengthening effect in particulate-reinforced metal matrix nanocomposites: A model for predicting their yield strength, *Scr. Mater.* 54(7) (2006) 1321-1326.

Figure captions

Figure 1. Schematic representation of accumulative fold forging process combined with the experimental samples.

Figure 2. FE-SEM images showing the layered structure of processed UFGed alloy and dispersion of precipitates.

Figure 3. (a, b) Bright- and (c, d) dark-field TEM images from the prepared FIB thinned foil sample across the thickness section.

Figure 4. Bright-field TEM images showing the ultra-fine grained structure of processed aluminum alloy across the thickness section.

Figure 5. Corresponding dark-field TEM images from the UFGed structure.

Figure 6. TEM images from the structure and morphology of precipitates within the alloy matrix at different regions.

Figure 7. (a) FIB-TEM grain structure image combined with the STEM EDS elemental analysis mapping results. (b) TEM image combined with the STEM elemental analysis mapping from the precipitates and deformed aluminum alloy matrix.

Figure 8. TEM images combined with the STEM EDS point scan analysis results from the aluminum alloy matrix and different precipitates.

Figure 9. Optical macro-graphs showing the testing points, indentation features and related hardness values for the processed UFGed layered aluminum alloy structure.

Figure 10. Indentation load-depth responses related to the different measurements.

Figure 11. (a) XRD pattern from the processed UFGed layered material. (b) Variation of $(\delta S)^2_{phy}$ versus S^2 for four diffraction peaks of (111), (200), (220) and (311).

Figure 12. (a, b) High magnification TEM images showing the gradual formation of UFG bands from dislocations. (c) Schematic representation from the formation of UFGed layered structure during AFF process.

Table 1. Chemical composition of the examined AA8006 aluminum alloy (*wt*%).

Element	Al	Mn	Si	Fe	Cu	Zn	Cr	Mg
AA8006	Base	0.55	0.25	1.24	0.01	0.02	<0.01	<0.01

Table 2. Contribution of different strengthening mechanisms on the Vickers hardness of processed UFGed layered structure from aluminum alloy.

Material	Experimental	Modeling					Deformation field effect
	$H_{\exp}$	H_0	H_{gb}	H_{dis}	H_{pp}	H_l	f_{dfe}
UFGed layered AA8006 alloy	61.5	4.3	32.9	6.4	9.1	8.8	2×10^{-6}

Research highlights:

- A novel SPD process named as AFF was introduced.
- AFF process is based on the repetitive forging of folded metal foils.
- This new method possesses an exceptional capability for fabrication of UFG layered structures.
- An AA8006 aluminum alloy layered material with the UFG structure of 200-300 nm was produced.
- An enhanced hardness up to ~100% was attained owing to the UFG and layered structures.

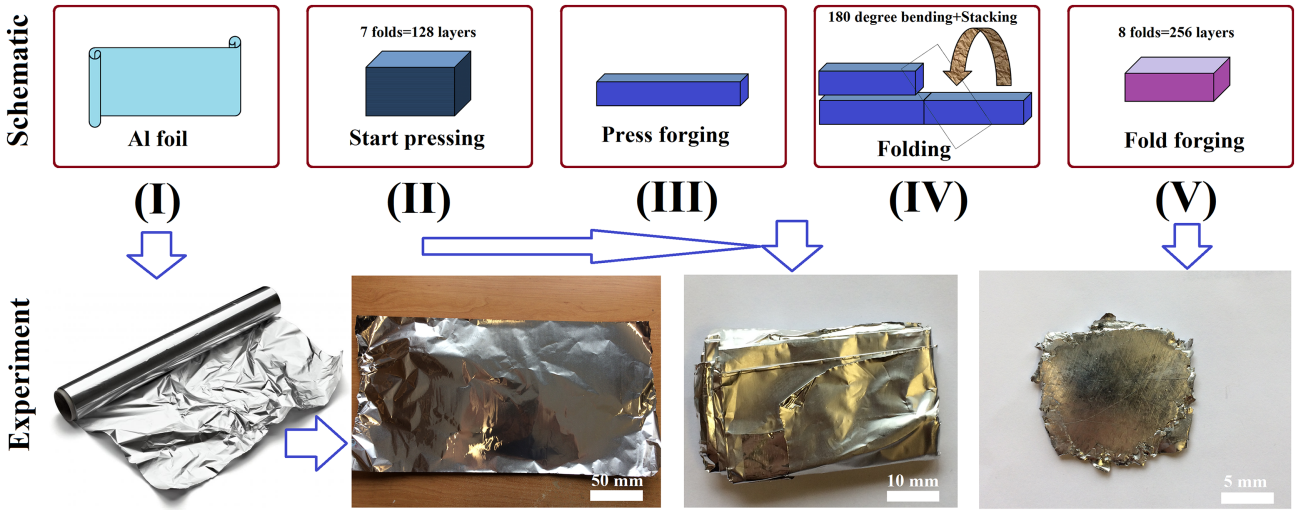
Schematic
Al foil
7 folds=128 layers
Start pressing
Press forging
180 degree bending+Stacking
Folding
8 folds=256 layers
Fold forging
(I)
(II)
(III)
(IV)
(V)
Experiment
50 mm
10 mm
5 mm

Figure 1

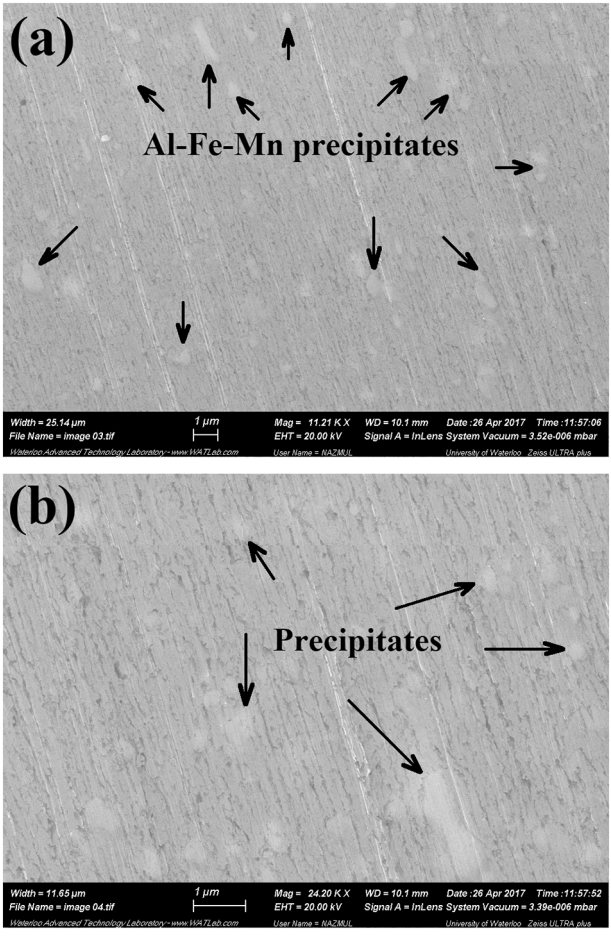
(a)
Al-Fe-Mn precipitates
Width = 25.14 µm
File Name = image 03.tif
1 µm
Mag = 11.21 K X
EHT = 20.00 kV
WD = 10.1 mm
Signal A = InLens
Date :26 Apr 2017
Time :11:57:06
System Vacuum = 3.52e-006 mbar
Waterloo Advanced Technology Laboratory - www.WATLab.com
User Name = NAZMUL
University of Waterloo Zeiss ULTRA plus
(b)
Precipitates
Width = 11.65 µm
File Name = image 04.tif
1 µm
Mag = 24.20 K X
EHT = 20.00 kV
WD = 10.1 mm
Signal A = InLens
Date :26 Apr 2017
Time :11:57:52
System Vacuum = 3.39e-006 mbar
Waterloo Advanced Technology Laboratory - www.WATLab.com
User Name = NAZMUL
University of Waterloo Zeiss ULTRA plus

Figure 2

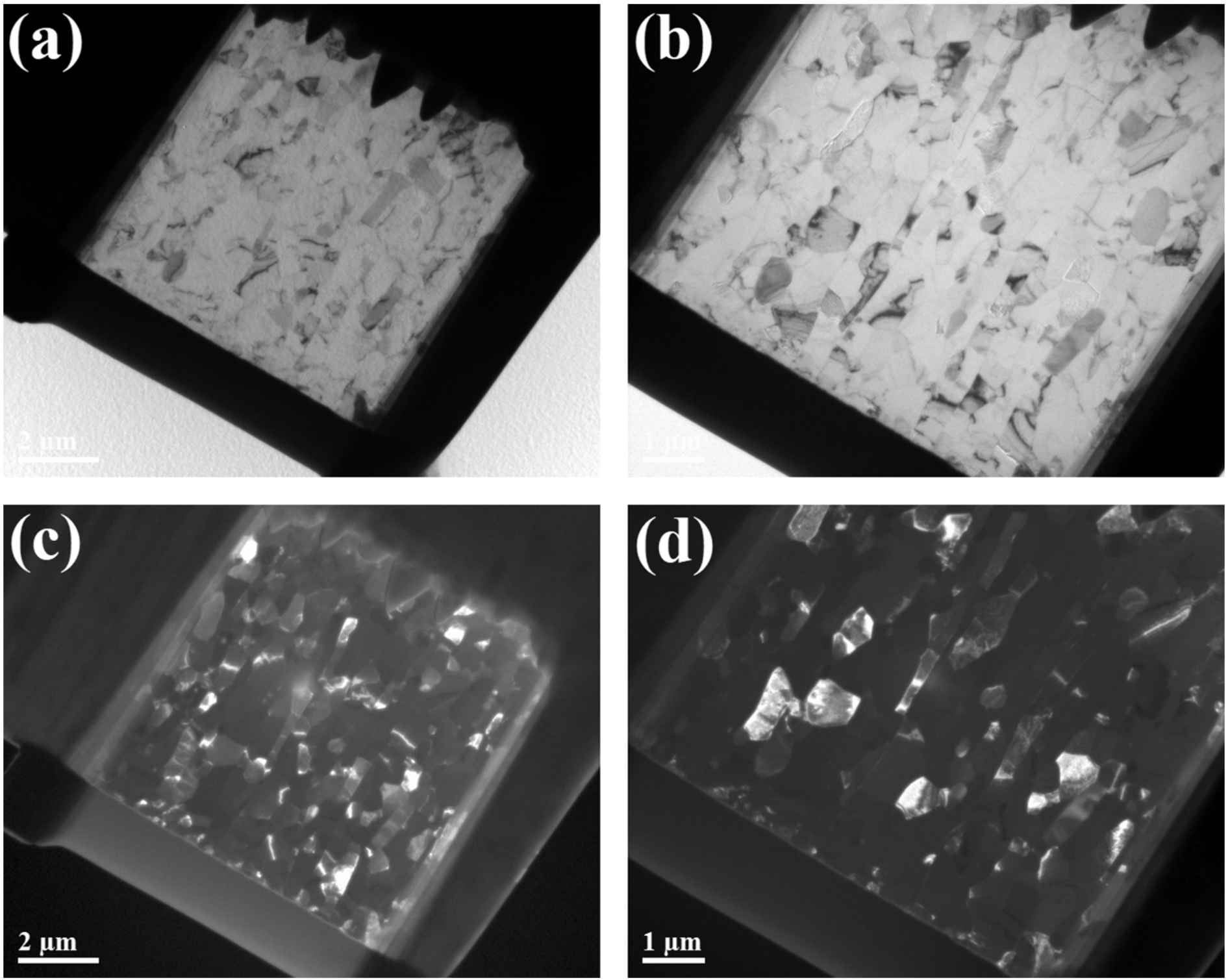

Figure 3

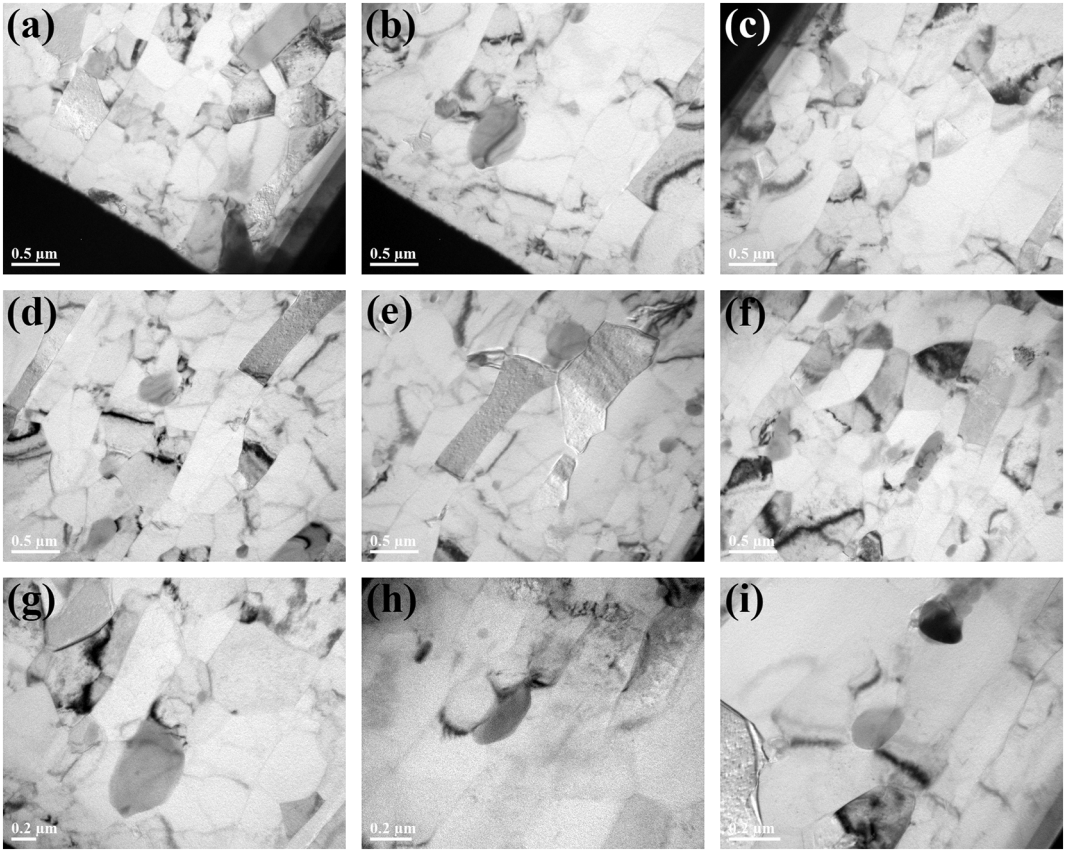

Figure 4

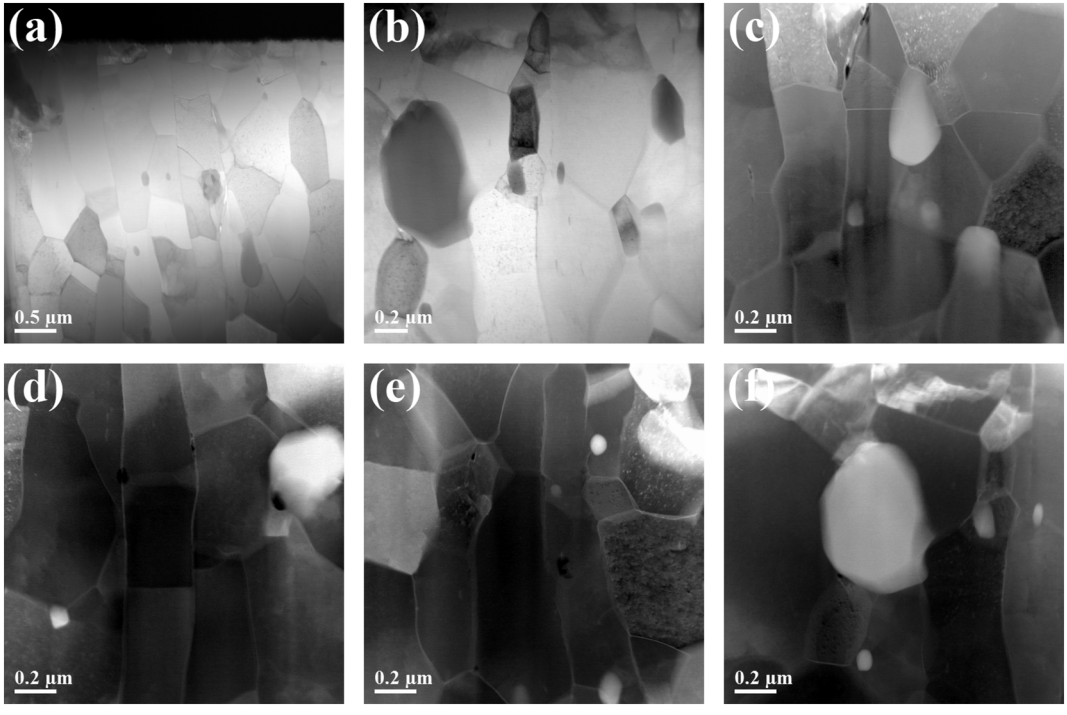

Figure 5

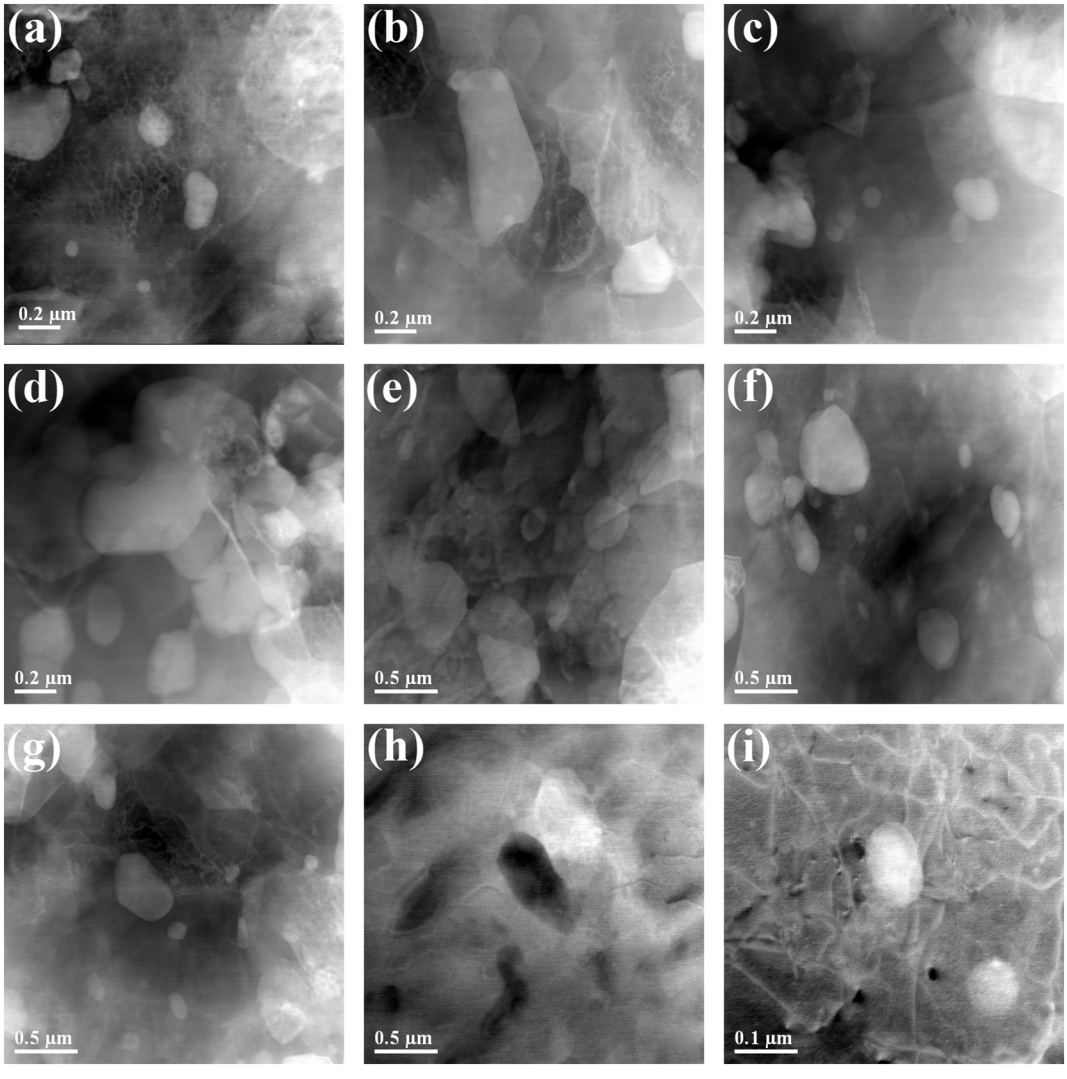

Figure 6

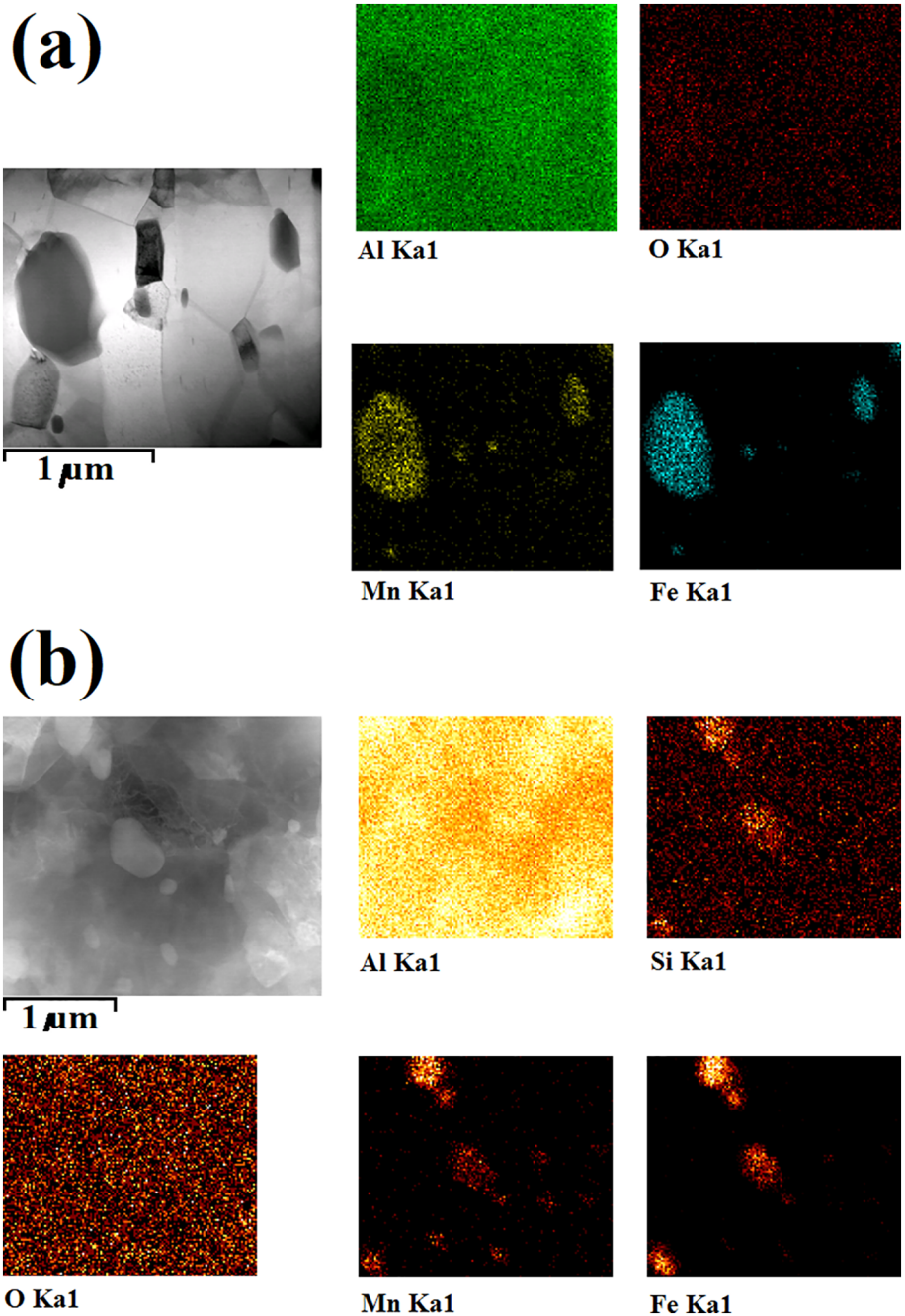
(a)
Al Ka1
O Ka1
1 μm
Mn Ka1
Fe Ka1
(b)
Al Ka1
Si Ka1
1 μm
O Ka1
Mn Ka1
Fe Ka1

Figure 7

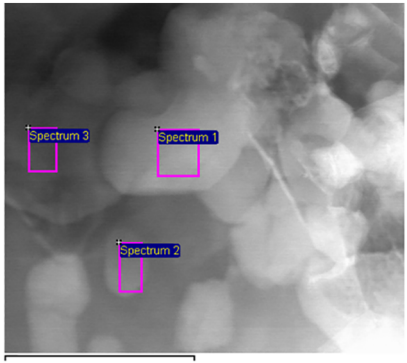
Spectrum 3
Spectrum 1
Spectrum 2
800 nm

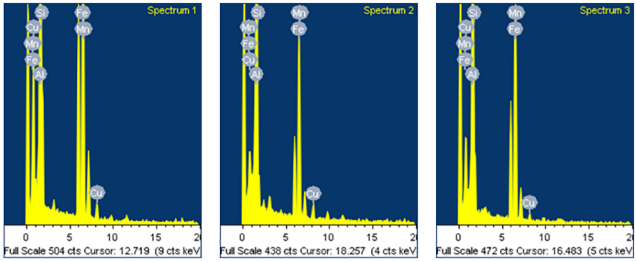
Spectrum 1
Full Scale 504 cts Cursor: 12.719 (9 cts keV
Spectrum 2
Full Scale 438 cts Cursor: 18.257 (4 cts keV
Spectrum 3
Full Scale 472 cts Cursor: 16.483 (5 cts keV

(a)

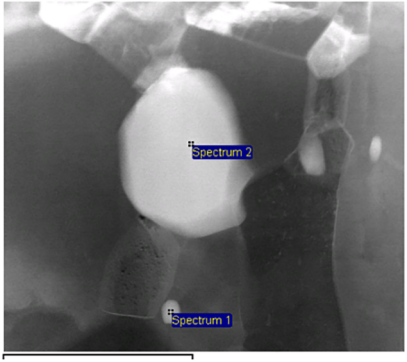
Spectrum 2
Spectrum 1
800 nm

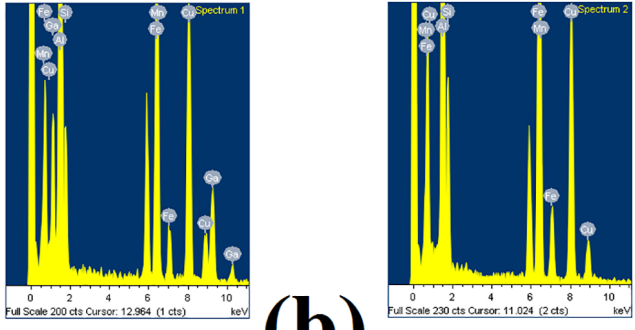
Spectrum 1
Full Scale 200 cts Cursor: 12.964 (1 cts)
keV
Spectrum 2
Full Scale 230 cts Cursor: 11.024 (2 cts)
keV

(b)

Figure 8

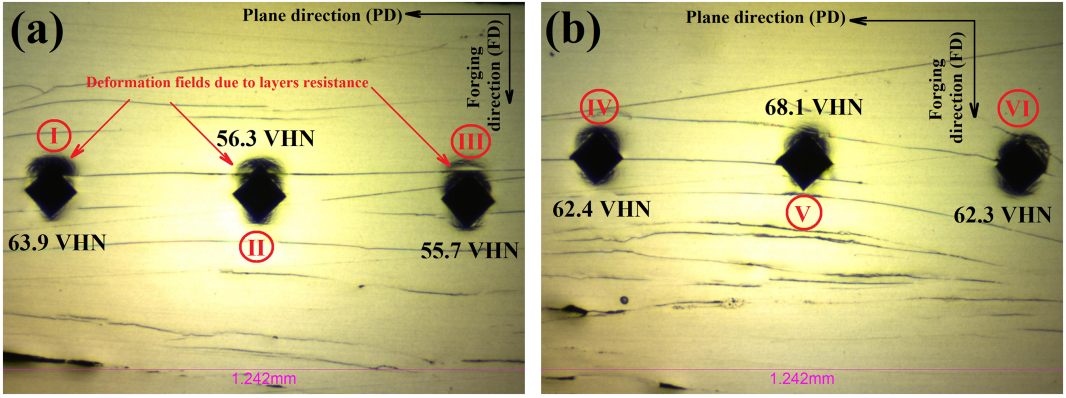
(a)
Plane direction (PD)
Forging direction (FD)
Deformation fields due to layers resistance
I
56.3 VHN
III
63.9 VHN
II
55.7 VHN
1.242mm
(b)
Plane direction (PD)
Forging direction (FD)
IV
68.1 VHN
VI
62.4 VHN
V
62.3 VHN
1.242mm

Figure 9

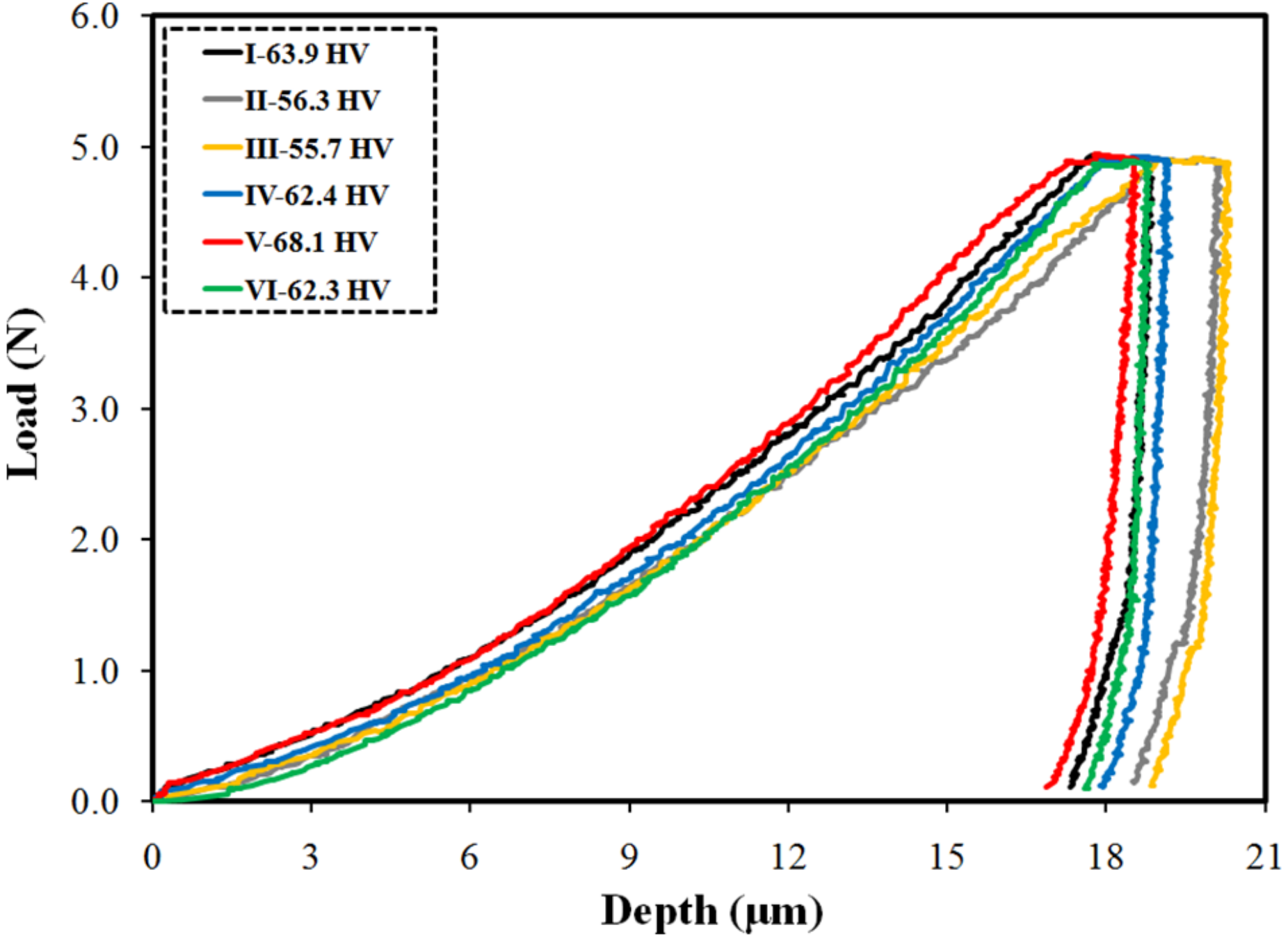
I-63.9 HV
II-56.3 HV
III-55.7 HV
IV-62.4 HV
V-68.1 HV
VI-62.3 HV
Load (N)
Depth (µm)
0.0
1.0
2.0
3.0
4.0
5.0
6.0
0
3
6
9
12
15
18
21

Figure 10

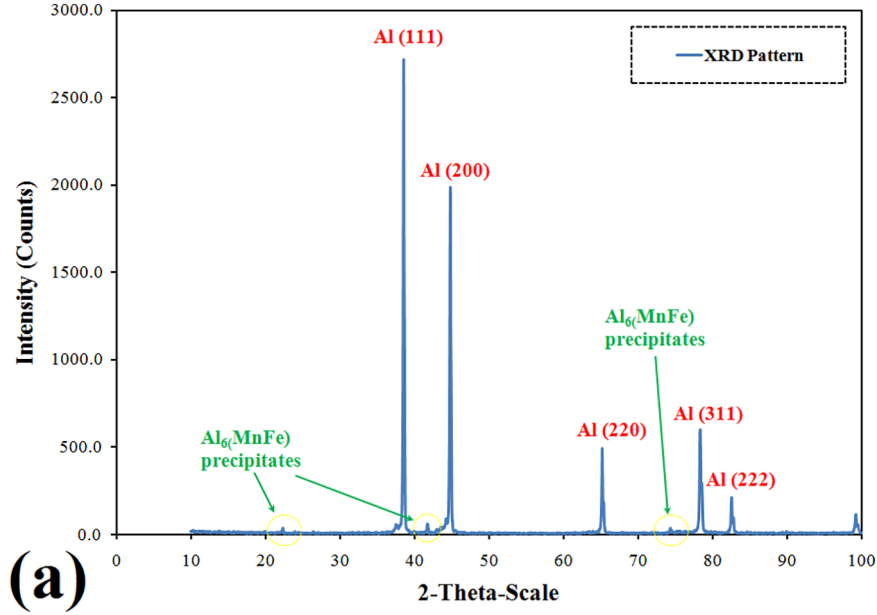
Al (111)
Al (200)
Al (220)
Al (311)
Al (222)
Al6(MnFe) precipitates
Al6(MnFe) precipitates
XRD Pattern
Intensity (Counts)
2-Theta-Scale
(a)

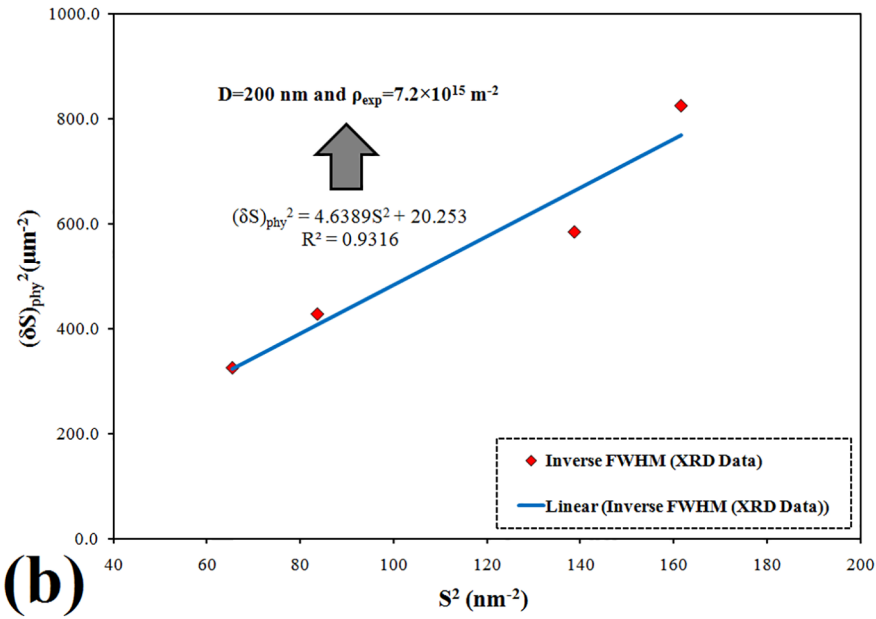
D=200 nm and ρexp=7.2×10^15 m^-2
(δS)phy^2 = 4.6389S^2 + 20.253
R² = 0.9316
Inverse FWHM (XRD Data)
Linear (Inverse FWHM (XRD Data))
(δS)phy^2 (μm^-2)
S² (nm^-2)
(b)

Figure 11

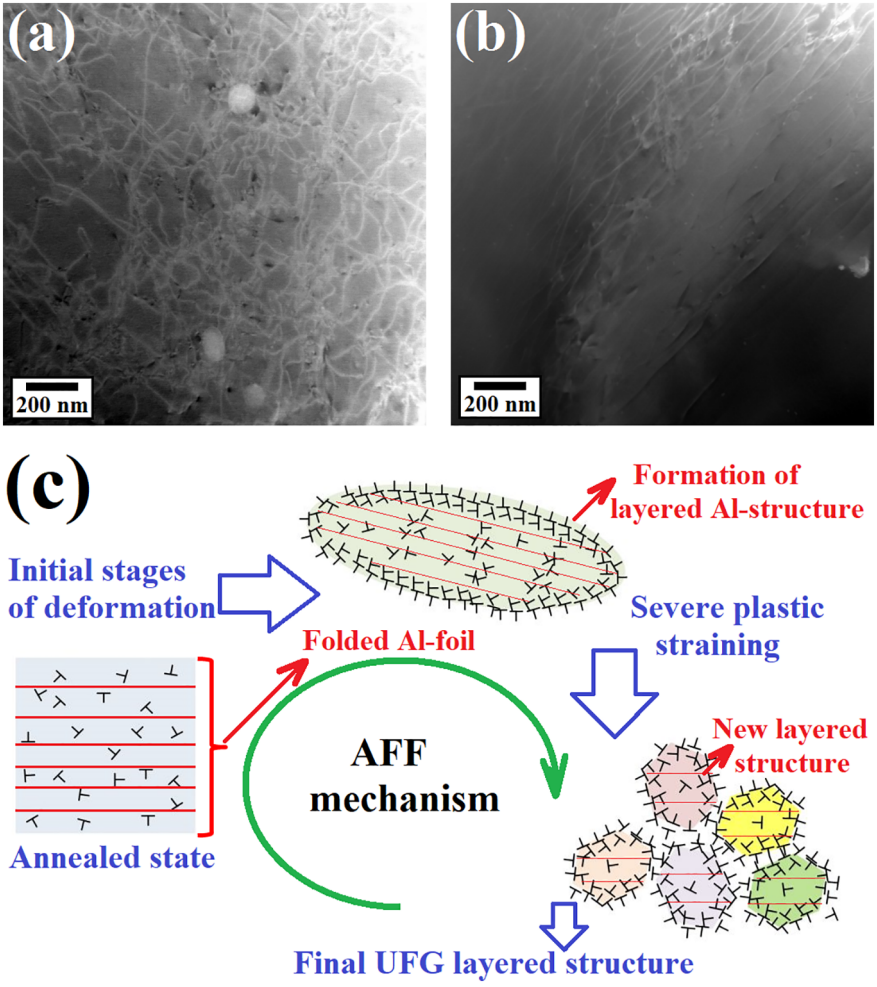
(a)
200 nm
(b)
200 nm
(c)
Formation of layered Al-structure
Initial stages of deformation
Severe plastic straining
Folded Al-foil
AFF mechanism
New layered structure
Annealed state
Final UFG layered structure

Figure 12